Research Article | Vol. 28, No. 7 / 30 March 2020 / Optics Express 9393
Optics EXPRESS

Ultra-low loss hybrid ITO/Si thermo-optic phase shifter with optimized power consumption

JORGE PARRA, JUAN HURTADO, AMADEU GRIOL, AND PABLO SANCHIS*

Nanophotonics Technology Center, Universitat Politècnica de València, Camino de Vera s/n, 46022 Valencia, Spain
**pabsanki@ntc.upv.es*

Abstract: Typically, materials with large optical losses such as metals are used as microheaters for silicon based thermo-optic phase shifters. Consequently, the heater must be placed far from the waveguide, which could come at the expense of the phase shifter performance. Reducing the gap between the waveguide and the heater allows reducing the power consumption or increasing the switching speed. In this work, we propose an ultra-low loss microheater for thermo-optic tuning by using a CMOS-compatible transparent conducting oxide such as indium tin oxide (ITO) with the aim of drastically reducing the gap. Using finite element method simulations, ITO and Ti based heaters are compared for different cladding configurations and TE and TM polarizations. Furthermore, the proposed ITO based microheaters have also been fabricated using the optimum gap and cladding configuration. Experimental results show power consumption to achieve a π phase shift of 10 mW and switching time of a few microseconds for a 50 μm long ITO heater. The obtained results demonstrate the potential of using ITO as an ultra-low loss microheater for high performance silicon thermo-optic tuning and open an alternative way for enabling the large-scale integration of phase shifters required in emerging integrated photonic applications.

1. Introduction

The ability to control the phase of the light is one of the most important features in silicon photonic integrated circuits (PICs). The most common way to induce a phase shift is by exploiting the silicon thermo-optic (TO) coefficient ($\sim 1.8 \times 10^{-4}$ K^{-1}) [1]. Thermo-optic tuning can be easily attained by heating the waveguide with a metallic microheater. Furthermore, this mechanism can be used with negligible optical losses by placing the lossy microheater at a certain distance from the waveguide. However, the heater is usually located far from the waveguide, which could lead to a low performance in terms of high power consumption or low switching speeds.

Thermo-optic phase shifters are used in a wide range of current and new integrated photonic applications such as phased arrays [2], neural networks [3], integration with nanoelectronics [4], reconfigurable photonics [5] or integrated quantum photonics [6]. However, most of the previous works focus on the the performance of the TO device using a metallic microheater [7–13]. On the other hand, the influence of the upper-cladding cladding material was investigated by Atabaki *et al.* [14] showing a trade-off between the power consumption and the switching speed. Hence, the most straightforward way to improve both parameters is to reduce the gap between the waveguide and the microheater.

Previous works have proposed 2D materials such as graphene as a transparent heater in order to reduce the gap [15–20]. However, graphene involves complex fabrications processes that are not yet prepared for large-scale and massive PICs production. In this scenario, CMOS-compatible transparent conducting oxides (TCOs) such as indium tin oxide (ITO) or Al-doped zinc oxide arise. These materials can be easily deposited with high quality in thin film by using various deposition methods such as atomic layer deposition [21], pulsed layer deposition [22] or RF/DC sputtering [23]. Transparent conducting oxides have been an increasingly object of interest

#386959 https://doi.org/10.1364/OE.386959
Journal © 2020 Received 27 Dec 2019; revised 14 Feb 2020; accepted 21 Feb 2020; published 18 Mar 2020

Optics EXPRESS

because their epsilon-near-zero (ENZ) regime in the near-infrared (near-IR) region of the spectrum [24]. In the field of PICs, this unique feature has been exploited to provide high performance electro-absorption devices [25–35], since optical losses are drastically enhanced in the ENZ regime. Nevertheless, if the TCO is biased far from the ENZ regime, this behaves as an optically transparent and electrically conducting material and thus, an ideal candidate for using as an ultra-low loss microheater.

In this work we propose, design and fabricate transparent ITO heaters for high performance TO tuning of silicon photonic structures. The ultra-low loss ITO heater is compared with a titanium based one for different cladding configurations. The influence of the spacer between the waveguide and the microheater is analyzed and the advantages of ITO against Ti are shown for TE and TM polarizations. Finally, ITO heaters are fabricated for a fully surrounded SiO_2 configuration and characterized for both polarizations using the optimal gaps found in the design section.

2. Design

2.1. Design methodology

Typical heater/Si waveguide configuration is depicted in Fig. 1(a). A metallic heater is placed on top of the silicon waveguide in order to induce a phase shift from the combination of Joule heating and the silicon TO coefficient. Because metals are high-loss in the near-IR, an upper-cladding is used to optically isolate the heater and the silicon waveguide. However, large spacers may suppose a drawback in the phase shifter performance such as the power consumption and/or the switching speed.

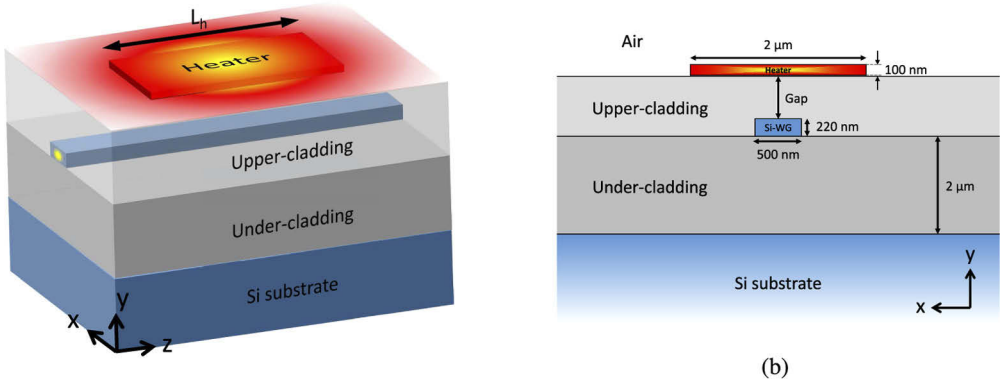

Fig. 1. (a) 3D view schematic and (b) cross-section of the analyzed heater/Si waveguide configuration.

Because the heater does not vary in the propagation direction of the light, the temperature in the silicon waveguide can be obtained by solving the following conductive heat equation for the cross-section (see Fig. 1(b)):

$$\nabla(-k\nabla T) + Dc\frac{\partial T}{\partial t} = Q \tag{1}$$

where k is the thermal conductivity, D the density, c the specific heat capacity, T the temperature, t the time and Q the heat source. This latter can be defined as:

$$Q = \frac{P}{V} \tag{2}$$

Optics EXPRESS

where P and V stand for the electrical power applied to the heater and the volume of the microheater, respectively. Doing some manipulations, the heat source can also be expressed as:

$$Q = \rho \frac{I^2}{S^2} \tag{3}$$

where ρ is the heater resistivity, I the current flowing through the heater and S the heater cross-section area. By using a low-conducting heater, the amount of current can be diminished, which can avoid self-heating problems of the heater driver system.

It has to be highlighted that the performance of the phase shifter does not depend with the heater length. The heater length, L_h, neglects when both heat ($\Delta\phi \propto \Delta n_{\text{eff}} \propto \Delta T \propto 1/L_h$) and optical phase shift ($\Delta\phi \propto L_h$) equations are combined. Hence, the same phase shift is induced for a given power consumption regardless the heater length [12]. Therefore, two strategies can be followed by either inducing a large (small) change in the effective refractive index with a short (long) heater. By assuming the steady state ($\partial T/\partial t = 0$), the power consumption can be then reduced either by diminishing the thermal conductivity of the cladding, for instance by using air trenches [7], or by narrowing and thinning the heater. However, both approaches have trade-offs. On one hand, reducing the thermal conductivity can improve the power consumption by an order of magnitude but switching times usually worsen in the same degree. On the other hand, reducing the heater cross-section may have some issues. A small cross-section will rise the current density and could melt the heater. Furthermore, the driving voltage will also be higher and a more stringent alignment will be required if the heater is narrowed to the same order of the waveguide width. Concerning the thickness, making homogeneous and high-quality thin films becomes hard for thicknesses lower than 100 nm. Consequently, in this work the heater width and thickness is set to 2 µm and 100 nm, respectively.

In contrast to metals, in which both optical and electrical properties cannot be tuned, ITO has the advantage of tuning them during the fabrication steps such as deposition or post-annealing [22,36,37]. The optical properties of ITO ($\varepsilon = \varepsilon' + j\varepsilon''$) in the near-IR are described by the Drude model:

$$\varepsilon = \varepsilon_\infty \left(1 - \frac{\omega_p^2}{\omega^2 + j\omega\Gamma}\right), \tag{4}$$

where ω stands for the angular frequency, ε_∞ is the high-frequency permittivity, Γ the damping factor and ω_p is the so-called plasma frequency. This latter defined as:

$$\omega_p = \sqrt{\frac{Nq^2}{\varepsilon_\infty \varepsilon_0 m^*}}, \tag{5}$$

where q is the elementary charge, m^* the electron effective mass and N the free carrier density. On the other hand, the resistivity ρ is obtained as:

$$\rho = \frac{\Gamma m^*}{Nq^2}. \tag{6}$$

In Fig. 2 is represented both permittivity ($\lambda = 1550$ nm) and resistivity of ITO as a function of the free carrier density. On one hand, a low-doped ITO ($N = 10^{19}$ cm^{-3}) provides both high-transparency ($\varepsilon'' \approx 0$) and high-resistivity properties. Below this value, ITO behaves as a Mott insulator and is no longer conducting [38]. On the other hand, the light-matter interaction is enhanced in the ENZ regime ($N = 6.5 \times 10^{20}$ cm^{-3}), where $\varepsilon' = 0$, $\varepsilon'' > 0$ and $|\varepsilon|$ achieves its minimum value ($|\varepsilon| = 0.57$). As a result, optical losses may be drastically increased and thus, the transparency condition is lost.

Therefore, an ITO free carrier concentration of 10^{19} cm^{-3} is chosen, which provides a refractive index of $1.960 + j2.3 \times 10^{-3}$ and a resistivity of 2.24×10^{-2} Ω cm. Heat and optical properties

Optics EXPRESS

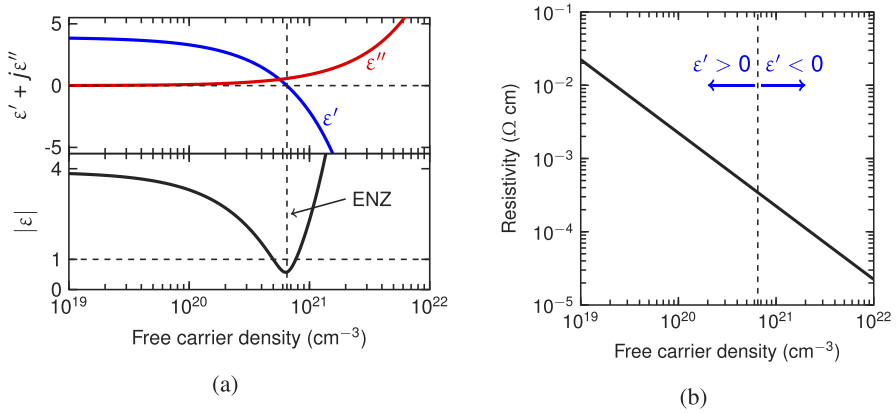

Fig. 2. (a) ITO permittivity and (b) resistivity as a function of the free carrier density. Permittivity is obtained by using the Drude model at $\lambda = 1550$ nm. Drude parameters are: $\varepsilon_\infty = 3.9$, $\Gamma = 1.8 \times 10^{14}$ rad/s and $m^*/m_e = 0.35$ [39].

used for simulations are shown in Table 1. It is worth mentioning that the imaginary part of the ITO refractive index is almost three orders of magnitude lower than Ti. This difference enables an ultra-low loss heater, which could be exploited to reduce the spacer with the silicon waveguide and thus, improve the performance of the phase shifter.

Table 1. Thermal and optical constants. Refractive index is given at 1550 nm.

	D (kg m^{-3})	c (J kg^{-1} K^{-1})	k (W m^{-1} K^{-1})	$n + j\kappa$
Si	2330	703	163	3.476
SiO_2	2203	650	1	1.444
SiN	2500	170	14	2
Ti	4500	523	23	$4.04 + j3.82$
ITO	7140	364	10	$1.960 + j2.3 \times 10^{-3}$

2.2. *Influence of the spacer on the power consumption and switching speed*

The influence of the gap for different under- and upper-claddings is analyzed comparing both Ti and ITO heaters. In this work, a low and high thermal conducting materials such as SiO_2 and SiN is chosen for the claddings. Temperature distribution and optical modes for TE and TM polarization are obtained by using finite element method.

Heat distribution for the steady-state in the cross-section for different under- and upper-cladding configurations is shown in Fig. 3. The gap between the heater and the waveguide is 1 µm and the heater temperature is fixed. It is worth mentioning that the value of the heater thermal conductivity is not relevant. Consequently, in terms of heat distribution and propagation, it is pointless which material is used as a heat source.

When both claddings have the same thermal conductivity (see Figs. 3(a) and 3(c)), heat spreads across the claddings with negligible difference. However, for the SiN/SiO_2 configuration (see Fig. 3(b)), the SiO_2 under-cladding acts as a thermal wall for the SiN upper-cladding. Hence, heat distribution is almost constant an more homogeneous in the upper-cladding for both y- and x-axis. Nonetheless, all configurations are robust to heater misalignment with respect to the waveguide in the x-axis of several hundreds of nanometers.

The power consumption of TO phase shifters is commonly assessed by the electrical power needed to achieve a phase shift of π rad (P_π). Figure 4(a) shows P_π as a function of the gap for

Optics EXPRESS

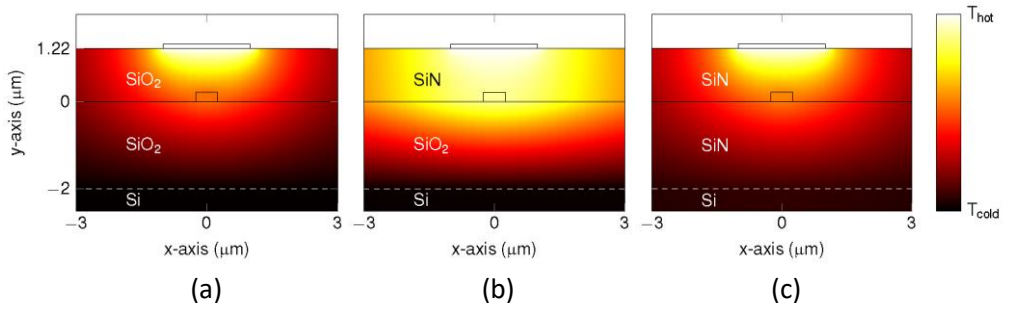

Fig. 3. Normalized steady-state heat distribution for different upper- and under-claddings. (a) SiO_2/SiO_2, (b) SiN/SiO_2 and (c) SiN/SiN.

the different cladding configurations and heaters and for TM polarization. Differences between Ti- and ITO-based heaters are negligible for gaps above 500 nm. Below it, hybrid-plasmonic modes begin to form for the Ti heater configuration whereas for the ITO heater remains photonic. For the SiN/SiO_2 claddings, the difference is more pronounced because the asymmetric cladding. This is depicted in Fig. 4(b), where optical modes for a gap of 200 and 500 nm are compared for both heaters. When the spacer between the heater and the waveguide is sufficiently large (500 nm), a photonic mode is excited for both cases. However, if both structures are close enough (200 nm), the Ti heater disallows the optical mode to be guided within the silicon waveguide and the light shifts towards the Ti because its $\varepsilon' < 0$, conversely to ITO. When no gap exists a plasmonic mode is obtained for the Ti heater since the mode is confined at the Si/Ti interface, whereas for the ITO heater remains guided within the silicon waveguide. This optical deconfinement from the silicon when the Ti is used as a heater results in an increase of the power consumption.

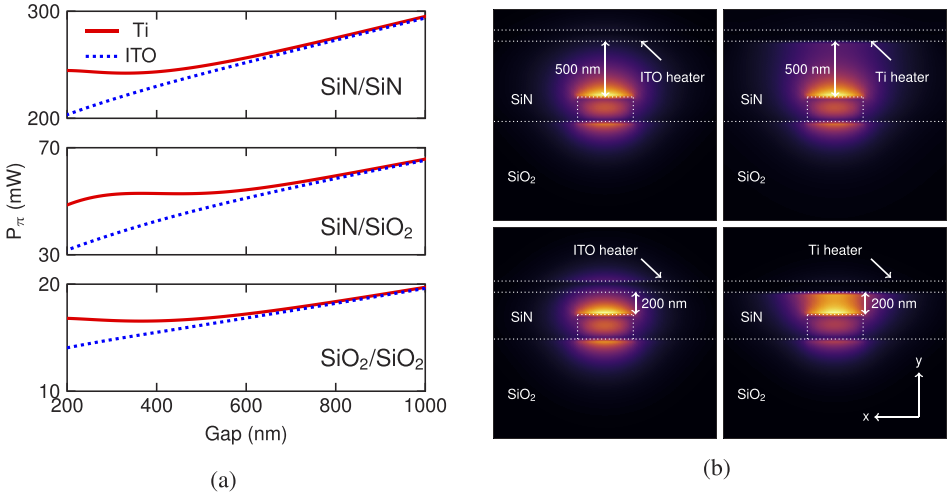

Fig. 4. (a) Power consumption (TM polarization) to achieve a phase shift of π rad (P_π) as a function of the gap for Ti (solid lines) and ITO (dashed lines) heaters and different under-/upper-claddings: SiO_2/SiO_2, SiN/SiO_2 and SiN/SiN. (b) Mode profile ($|E_y|$) comparison between ITO and Ti heater for the SiN/SiO_2 configuration and gaps of 200 and 500 nm. Results are obtained at $\lambda = 1550$ nm.

For TE polarization, power consumption ranges between 8-11 mW (SiO_2/ SiO_2), 19-32 mW (SiN/SiO_2) and 120-165 mW (SiN/SiN) with a linear relation with the gap for all cladding

Optics EXPRESS

configurations. The SiO_2/SiO_2 configuration remains as the one with lowest power consumption and dependence with the gap is also reduced. Furthermore, P_π is diminished in all cases with respect to TM polarization because of the higher confinement of light in the silicon waveguide.

Although a full SiO_2 cladding provides the lowest power consumption, its low thermal conductivity could be a drawback in terms of switching speed. The switching speed τ is evaluated by calculating the temporal response (Eq. (1)) of the phase shifter when applying a step electrical signal to the heater. In the present work, τ is defined as the time difference between the amplitude from 10% ($\tau_{10\%}$) to 90% ($\tau_{90\%}$). Maximum switching speed can be then calculated by obtaining either the rise or fall time of the phase shifter temporal response.

Figure 5 shows the switching speed for the different cladding configurations. A SiN upper-cladding results in an independent behaviour of the rise/fall times with the gap because of the SiN high thermal conductivity. Furthermore, the switching speed can be improved below the microsecond by using a full SiN cladding and avoiding the SiO_2 thermal wall. Conversely, a full SiO_2 cladding shows a high dependence of the switching speed with the gap because of the low thermal conductivity of the SiO_2 upper-cladding. Despite this fact, a full SiO_2 cladding is preferred due to the much lower power consumption, as shown in Fig. 4(a). Furthermore, low values of switching speed could also be attained if the gap is small enough, though optical losses induced by the heater impose a trade-off.

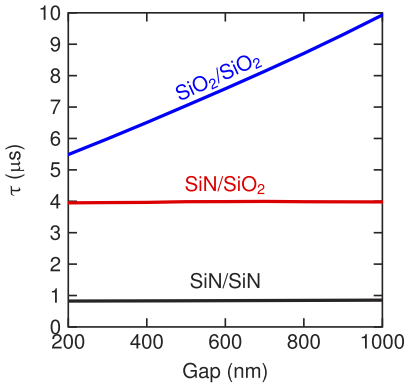

Fig. 5. Switching time as a function of the gap for the different under- and upper-claddings.

The minimum attainable gap is then imposed by the coupling losses that arise by the possible mismatch between the silicon waveguide and the phase-shifter. Figure 6(a) shows the total (input + output) coupling losses as a function of the gap for both polarizations and heaters. Coupling losses are obtained as the overlap of the optical modes with and without heater. For TE polarization, gaps greater than 200 nm suffice for both materials assuring coupling losses below 0.01 dB. Conversely, for TM polarization, the minimum gap needs to be increased up to 330 nm (ITO) and 630 nm (Ti).

On the other hand, the heater length for a given gap is constrained between an under- and upper-limit. The first is associated with the maximum thermal cross-talk allowed between adjacent silicon structures, whereas the maximum length is determined by the propagation losses (see Fig. 6(b)). In this work, the thermal cross-talk is set by fixing the heater maximum temperature at 100 °C [40]. Table 2 summarizes the best results achieved for ensuring insertion losses below 0.01 dB. Such low insertion losses are mandatory to allow massive integration of phase shifters. The optimization of the phase shifter parameters was carried out to achieve best performance and meeting both optical and thermal requirements by minimizing the gap. It can be seen that smaller gaps can be achieved for ITO because propagation losses are three orders of

Optics EXPRESS

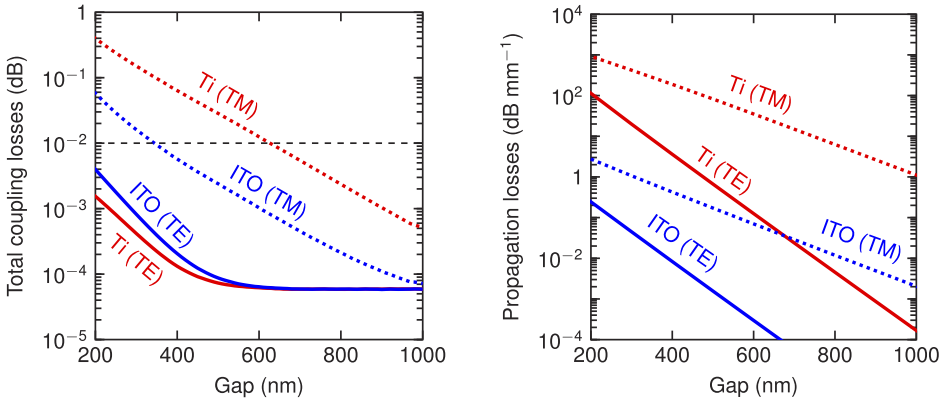

Fig. 6. (a) Coupling and (b) propagation losses as a function of the gap for a full SiO_2 cladding and for Ti and ITO heaters. Dashed line in (a) represents the limit of 0.01 dB.

magnitude lower than Ti, as depicted in Fig. 6(b). Therefore, such smaller gaps benefit the power consumption and switching time of the phase shifter

Table 2. Main results of ITO and Ti heaters to obtain less than 0.01 dB of insertion losses for the SiO_2/SiO_2 cladding configuration.

	Polarization	Gap (nm)	P_π (mW)	τ (µs)	L_h (µm)
ITO	TE	320	8.5	6.1	70
ITO	TM	660	17.2	7.9	145
Ti	TE	700	9.9	8.1	85
Ti	TM	1500	23.1	13.3	225

3. Experimental results

In Fig. 7(a) is shown an optical image of the fabricated structures used to validate the performance of the proposed hybrid ITO/Si phase shifter. Light was coupled to/from the optical fibers by using grating couplers for TE and TM polarization. Asymmetric Mach-Zehnder interferometers (MZIs) were used to extract the phase shift induced by the hybrid ITO/Si waveguide. Furthermore, 50 µm and 150 µm long ITO heaters were tested in order to investigate the influence of the heater length. Finally, ITO pads were also used to electrically contact the heater to the probes.

3.1. Fabrication

The silicon photonic structures were firstly fabricated by e-beam lithography and reactive ion etching (ICP/RIE) on silicon-on-insulator (SOI). Two copies in different samples were made and each one was covered with a target thickness of 320 nm and 660 nm SiO_2 upper-cladding, respectively, by plasma-enhanced chemical vapour deposition (PECVD). The measured experimental thicknesses were 312 nm and 660 nm. Finally, 2 µm wide and 100 nm thick ITO heaters were deposited on top of the upper-cladding. The ITO layer was deposited by DC sputtering in ArO_2 atmosphere. A post-annealing process was carried out for 30 minutes in a tubular oven in a forming gas (4% H_2 in Ar) atmosphere at 600 °C.

Optics EXPRESS

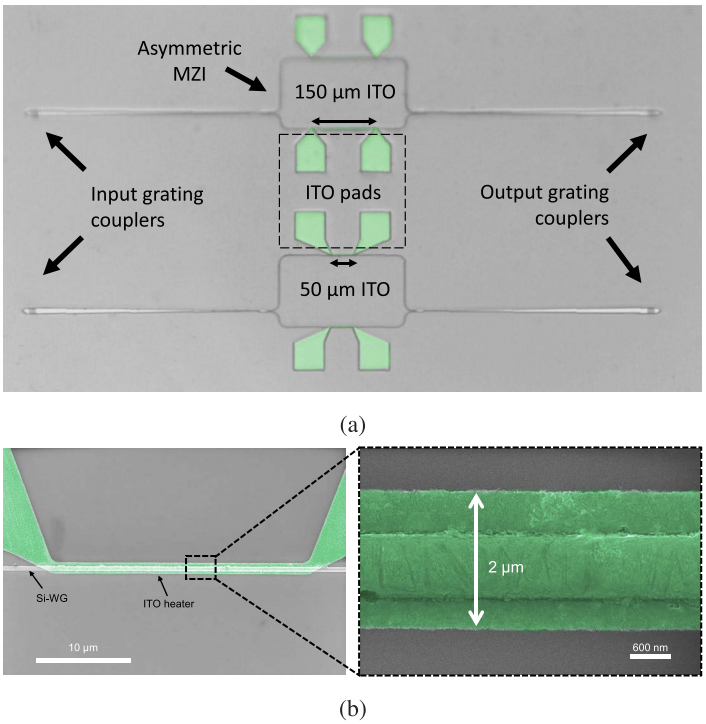

Fig. 7. (a) Optical image of the fabricated MZIs with ITO heaters on top. (b) SEM images of the ITO/Si TO phase shifter structure. The silicon waveguide looks wider than 500 nm because of the conformal PECVD deposition of the SiO_2 upper-cladding. On both images ITO is false coloured.

3.2. *Thermo-optic characterization*

Measured optical losses of the ITO/Si phase shifter were negligible in agreement with simulations (< 0.01 dB). In Fig. 8(a) is shown the normalized measured spectrum of the TE MZI with 50 µm long heaters on-top for zero power consumption and P_π. During measurements, sharp resonances with extinction ratios larger than 20 dB were achieved, which allowed to accurately estimate the power consumption.

In Fig. 8(b) is depicted the experimental phase shift $\Delta\phi$ as a function of the power consumption of the 150 µm long heater for TE and TM polarization. The P_π is then obtained by linearly fitting the experimental results. For both polarizations the resulting experimental P_π is in very good agreement with simulations. TE polarization shows $P_\pi = 9.7$ mW, whereas for TM a P_π of 20.2 mW is obtained.

The influence of the heater length on the power consumption for TE polarization is shown in Fig. 8(c). The same behaviour was achieved for TM polarization. As it can be noticed, the influence of the heater length is negligible on the value of the P_π. Small difference between both heaters are attributed to lower relation between the heater and pads resistance for the shortest heater, which leads to some power dissipation on the pads. The utilization of a shorter heater would permit to increase the density of phase shifters within the PIC. Furthermore, the driving voltage is reduced, going from 14.5 V (150 µm) to 9.1 V (50 µm).

The switching times of the phase shifter were obtained by biasing the MZI in the linear region. In Fig. 9(a) is depicted the recorded rise and fall times (312 nm upper-cladding) as a function of the applied power when a 10 kHz square signal was applied. For the 312 nm thick upper-cladding

Optics EXPRESS

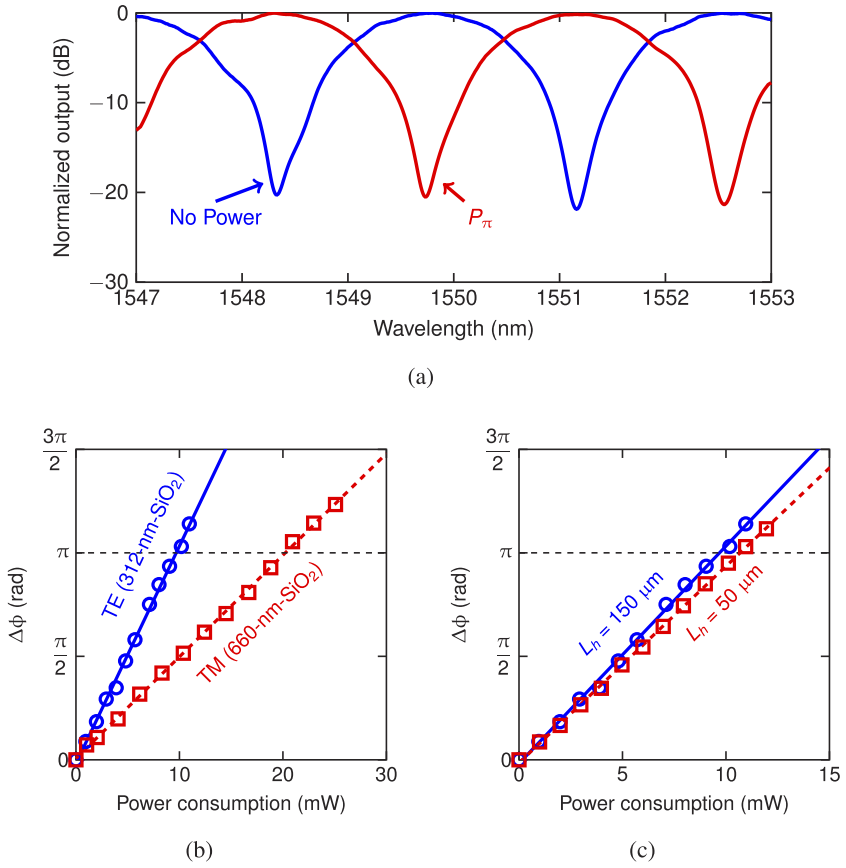

Fig. 8. (a) Normalized measured spectrum of the TE MZI with 50 μm long ITO heaters on-top for zero and P_π power applied to the heater on the long arm. Phase shift as a function of the ITO heater power consumption. (b) TE and TM polarization for a 150 μm long ITO heater. (c) TE polarization for a 150 μm and 50 μm long ITO heater.

(TE) a switching time of 5.2 μs was obtained, whereas for the 660 nm thick one (TM) was 6.8 μs. These differences between both switching times are due to the different gap value (see Fig. 5) and are in good agreement with the ones obtained in simulation. For small peak powers both rise and fall times are equal in agreement with the heating/cooling behaviour of a TO phase shifter. However, as the applied power is increased, the nonlinear regions of the MZI optical response affect the switching times [40]. Hence, both times diverges, and the resulting speed does not correspond to the hybrid ITO/Si phase shifter. This effect can be seen in Figs. 9(b) and 9(c). In the first case, a small amount of electrical power is applied and thus, the MZI swings in the linear region leading to equal rise and fall times. However, in Fig. 9(c), the peak power falls within the nonlinear region of the MZI. Consequently, both rise and fall times do not correspond only to the phase shifter but the combinations of the nonlinear response of the MZI with the phase shifter.

3.3. Discussion and state-of-the-art comparison

The focus of this work has been to optimize the performance of a TO phase shifter based on a standard silicon waveguide. A recent comparison of TO phase shifters based on silicon waveguides has been recently reported by M. Jacques et al. [12]. Metal heaters on-top of the silicon waveguide and approaches based on doping the silicon waveguide are compared by

Optics EXPRESS

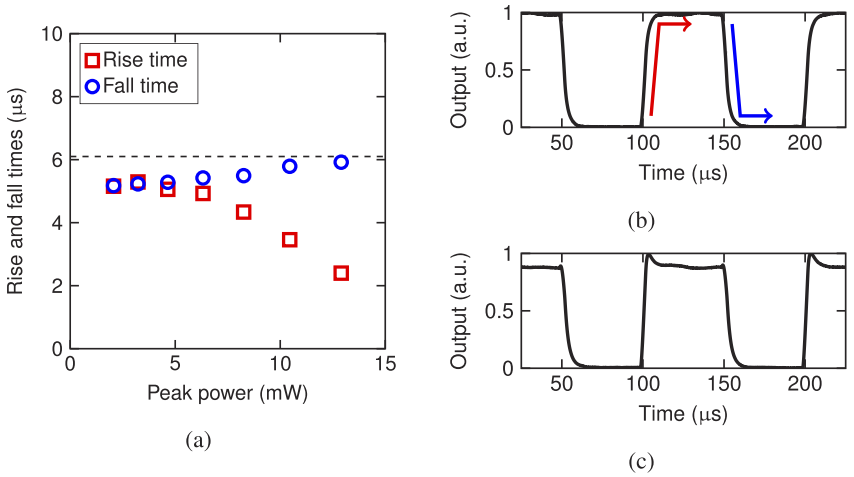

Fig. 9. (a) Recorded rise and fall times when a 10 kHz square signal is applied to the heater as a function peak power power applied to the heater. Dashed line stands for simulation value. Normalized temporal response when (a) 4 mW and (b) 13 mW of peak power is applied to the heater. Measurements correspond for TE polarization and a 50 μm long ITO heater.

using the figure of merit (FOM) of $P_\pi \tau$. The TO phase shifter of the present work achieves a experimental FOM of 52 mW μs for TE polarization, outperforming all the works compared in [12]. Furthermore, the insertion losses of our device are also significantly smaller (< 0.01 dB) and the FOM is almost one of order of magnitude better than in TO phase shifters reported by A. Massod et al. [9].

Such vale of FOM is achieved by reducing the gap between the heater and the silicon waveguide thanks of the ITO properties which minimizes absorption losses. Graphene has also such advantage. However, as point out in the introduction, the integration of ITO is currently more suitable for large-scale and massive PICs production. A slightly better FOM of ~ 36 mW μs was demonstrated on a TO phase-shifter based on using graphene as heater on-top of the silicon waveguide [16]. However, upper-cladding was based on two different layers of HSQ and Al_2O_3, which is different from the more standard SiO_2 upper-cladding. Furthermore, the TO phase shifter was based on a rib waveguide and measured at 1310 nm. In this sense, a FOM as low as ~ 2.5 mW μs for TE polarization has also been demonstrated by placing the graphene heater directly on-top of the waveguide [17]. However, the photonic waveguide was based on a photonic crystal designed to enhance the light-matter interaction by means of the slow-wave effect. Furthermore, high insertion losses of 1.1 dB were reported for the fabricated 20 μm long phase shifter (see Ref. [17] Supplementary).

4. Conclusions

In this work, a hybrid ITO/Si TO phase shifter have been proposed, designed and experimentally demonstrated by using a low-doped ITO as a microheater for TE and TM polarization. The main benefit of using ITO as heater is that up to 3 orders of magnitude lower optical losses can be achieved in comparison with typical metals such as titanium. In such a way, the gap between the heater and waveguide can be reduced which improves the performance of the phase shifter in terms of power consumption, switching speed and footprint. Experimental results show power consumption of 10 mW and switching times in order of the microsecond for a 50 μm long ITO heater. These results could open a new way for the large-scale integration of ultra-low loss phase shifters, which is critical in a wide range of emerging integrated photonic applications.

Optics EXPRESS

Funding

Ministerio de Economía y Competitividad (TEC2016-76849); Generalitat Valenciana (PROMETEO/2019/123); Ministerio de Ciencia, Innovación y Universidades (FPU17/04224).

Acknowledgements

The authors thank David Zurita for his help with the experimental set-up.

Disclosures

The authors declare no conflicts of interest.

References

1. J. Komma, C. Schwarz, G. Hofmann, D. Heinert, and R. Nawrodt, "Thermo-optic coefficient of silicon at 1550 nm and cryogenic temperatures," Appl. Phys. Lett. **101**(4), 041905 (2012).
2. E. Timurdogan, M. R. Watts, E. S. Hosseini, A. Yaacobi, and J. Sun, "Large-scale nanophotonic phased array," Nature **493**(7431), 195–199 (2013).
3. Y. Shen, N. C. Harris, D. Englund, and M. Soljacic, "Deep learning with coherent nanophotonic circuits," Nat. Photonics **11**(7), 441–446 (2017).
4. A. H. Atabaki, S. Moazeni, F. Pavanello, H. Gevorgyan, J. Notaros, L. Alloatti, M. T. Wade, C. Sun, S. A. Kruger, H. Meng, K. Al Qubaisi, I. Wang, B. Zhang, A. Khilo, C. V. Baiocco, M. A. Popović, V. M. Stojanović, and R. J. Ram, "Integrating photonics with silicon nanoelectronics for the next generation of systems on a chip," Nature **556**(7701), 349–354 (2018).
5. D. Pérez, I. Gasulla, L. Crudgington, D. J. Thomson, A. Z. Khokhar, K. Li, W. Cao, G. Z. Mashanovich, and J. Capmany, "Multipurpose silicon photonics signal processor core," Nat. Commun. **8**(1), 636 (2017).
6. J. Wang, F. Sciarrino, A. Laing, and M. G. Thompson, "Integrated photonic quantum technologies," Nat. Photonics (2019).
7. P. Sun and R. M. Reano, "Submilliwatt thermo-optic switches using free-standing silicon-on-insulator strip waveguides," Opt. Express **18**(8), 8406 (2010).
8. A. H. Atabaki, A. A. Eftekhar, S. Yegnanarayanan, and A. Adibi, "Sub-100-nanosecond thermal reconfiguration of silicon photonic devices," Opt. Express **21**(13), 15706 (2013).
9. A. Masood, M. Pantouvaki, G. Lepage, P. Verheyen, J. Van Campenhout, P. Absil, D. Van Thourhout, and W. Bogaerts, "Comparison of heater architectures for thermal control of silicon photonic circuits," *IEEE Int. Conf. on Group IV Photonics GFP* 2, 83–84 (2013).
10. A. Masood, M. Pantouvaki, D. Goossens, G. Lepage, P. Verheyen, J. Van Campenhout, P. Absil, D. Van Thourhout, and W. Bogaerts, "Fabrication and characterization of CMOS-compatible integrated tungsten heaters for thermo-optic tuning in silicon photonics devices," Opt. Mater. Express **4**(7), 1383 (2014).
11. Á. Rosa, A. Gutiérrez, A. Brimont, A. Griol, and P. Sanchis, "High performace silicon 2x2 optical switch based on a thermo-optically tunable multimode interference coupler and efficient electrodes," Opt. Express **24**(1), 191 (2016).
12. M. Jacques, A. Samani, E. El-Fiky, D. Patel, Z. Xing, and D. V. Plant, "Optimization of thermo-optic phase-shifter design and mitigation of thermal crosstalk on the SOI platform," Opt. Express **27**(8), 10456 (2019).
13. X. I. W. Ang and K. S. Chiang, "Polarization-insensitive mode-independent thermo-optic switch based on symmetric waveguide directional coupler," Opt. Express **27**(24), 35385–35393 (2019).
14. A. H. Atabaki, E. Shah Hosseini, A. A. Eftekhar, S. Yegnanarayanan, and A. Adibi, "Optimization of metallic microheaters for high-speed reconfigurable silicon photonics," Opt. Express **18**(17), 18312 (2010).
15. L. Yu, Y. Yin, Y. Shi, D. Dai, and S. He, "Thermally tunable silicon photonic microdisk resonator with transparent graphene nanoheaters," Optica **3**(2), 159 (2016).
16. D. Schall, M. Mohsin, A. A. Sagade, M. Otto, B. Chmielak, S. Suckow, A. L. Giesecke, D. Neumaier, and H. Kurz, "Infrared transparent graphene heater for silicon photonic integrated circuits," Opt. Express **24**(8), 7871 (2016).
17. S. Yan, X. Zhu, L. H. Frandsen, S. Xiao, N. A. Mortensen, J. Dong, and Y. Ding, "Slow-light-enhanced energy efficiency for graphene microheaters on silicon photonic crystal waveguides," Nat. Commun. **8**(1), 14411 (2017).
18. Z. Xu, C. Qiu, Y. Yang, Q. Zhu, X. Jiang, Y. Zhang, W. Gao, and Y. Su, "Ultra-compact tunable silicon nanobeam cavity with an energy-efficient graphene micro-heater," Opt. Express **25**(16), 19479 (2017).
19. J. Lv, Y. Yang, B. Lin, Y. Cao, Y. Zhang, S. Li, Y. Yi, F. Wang, and D. Zhang, "Graphene-embedded first-order mode polymer Mach-Zender interferometer thermo-optic switch with low power consumption," Opt. Lett. **44**(18), 4606 (2019).
20. X. Wang, W. Jin, Z. Chang, and K. S. Chiang, "Buried graphene electrode heater for a polymer waveguide thermo-optic device," Opt. Lett. **44**(6), 1480 (2019).
21. D. J. Lee, H. M. Kim, J. Y. Kwon, H. Choi, S. H. Kim, and K. B. Kim, "Structural and electrical properties of atomic layer deposited Al-doped ZnO films," Adv. Funct. Mater. **21**(3), 448–455 (2011).

Optics EXPRESS

22. J. W. Cleary, E. M. Smith, K. D. Leedy, G. Grzybowski, and J. Guo, "Optical and electrical properties of ultra-thin indium tin oxide nanofilms on silicon for infrared photonics," Opt. Mater. Express **8**(5), 1231 (2018).
23. S. Ray, R. Banerjee, N. Basu, A. K. Batabyal, and A. K. Barua, "Properties of tin doped indium oxide thin films prepared by magnetron sputtering," J. Appl. Phys. **54**(6), 3497–3501 (1983).
24. V. E. Babicheva, N. Kinsey, G. V. Naik, M. Ferrera, A. V. Lavrinenko, V. M. Shalaev, and A. Boltasseva, "Towards CMOS-compatible nanophotonics: Ultra-compact modulators using alternative plasmonic materials," Opt. Express **21**(22), 27326 (2013).
25. V. J. Sorger, N. D. Lanzillotti-Kimura, R. M. Ma, and X. Zhang, "Ultra-compact silicon nanophotonic modulator with broadband response," Nanophotonics **1**(1), 17–22 (2012).
26. K. Shi, R. R. Haque, B. Zhao, R. Zhao, and Z. Lu, "Broadband electro-optical modulator based on transparent conducting oxide," Opt. Lett. **39**(17), 4978 (2014).
27. C. Hoessbacher, Y. Fedoryshyn, A. Emboras, A. Melikyan, M. Kohl, D. Hillerkuss, C. Hafner, and J. Leuthold, "The plasmonic memristor: a latching optical switch," Optica **1**(4), 198 (2014).
28. X. Liu, K. Zang, J. H. Kang, J. Park, J. S. Harris, P. G. Kik, and M. L. Brongersma, "Epsilon-Near-Zero Si Slot-Waveguide Modulator," ACS Photonics **5**(11), 4484–4490 (2018).
29. E. Li, Q. Gao, R. T. Chen, and A. X. Wang, "Ultracompact Silicon-Conductive Oxide Nanocavity Modulator with 0.02 Lambda-Cubic Active Volume," Nano Lett. **18**(2), 1075–1081 (2018).
30. E. Li, Q. Gao, S. Liverman, and A. X. Wang, "One-volt silicon photonic crystal nanocavity modulator with indium oxide gate," Opt. Lett. **43**(18), 4429–4432 (2018).
31. R. Amin, R. Maiti, C. Carfano, Z. Ma, M. H. Tahersima, Y. Lilach, D. Ratnayake, H. Dalir, and V. J. Sorger, "0.52 V mm ITO-based Mach-Zehnder modulator in silicon photonics," APL Photonics **3**(12), 126104 (2018).
32. Q. Gao, E. Li, and A. X. Wang, "Ultra-compact and broadband electro-absorption modulator using an epsilon-near-zero conductive oxide," Photonics Res. **6**(4), 277 (2018).
33. M. G. Wood, S. Campione, S. Parameswaran, T. S. Luk, J. R. Wendt, D. K. Serkland, and G. A. Keeler, "Gigahertz speed operation of epsilon-near-zero silicon photonic modulators," Optica **5**(3), 233 (2018).
34. E. Li, B. A. Nia, B. Zhou, and A. X. Wang, "Transparent conductive oxide-gated silicon microring with extreme resonance wavelength tunability," Photonics Res. **7**(4), 473 (2019).
35. J. Parra, I. Olivares, A. Brimont, and P. Sanchis, "Non-volatile epsilon-near-zero readout memory," Opt. Lett. **44**(16), 3932 (2019).
36. Y. Gui, M. Miscuglio, Z. Ma, M. H. Tahersima, S. Sun, R. Amin, H. Dalir, and V. J. Sorger, "Towards integrated metatronics: a holistic approach on precise optical and electrical properties of Indium Tin Oxide," Sci. Rep. **9**(1), 11279 (2019).
37. S. Xian, L. Nie, J. Qin, T. Kang, C. Li, J. Xie, L. Deng, and L. Bi, "Effect of oxygen stoichiometry on the structure, optical and epsilon-near-zero properties of indium tin oxide films," Opt. Express **27**(20), 28618 (2019).
38. P. P. Edwards, A. Porch, M. O. Jones, D. V. Morgan, and R. M. Perks, "Basic materials physics of transparent conducting oxides," Dalton Transactions pp. 2995–3002 (2004).
39. F. Michelotti, L. Dominici, E. Descrovi, N. Danz, and F. Menchini, "Thickness dependence of surface plasmon polariton dispersion in transparent conducting oxide films at 1.55 μm," Opt. Lett. **34**(6), 839 (2009).
40. X. Fang and L. Yang, "Thermal effect analysis of silicon microring optical switch for on-chip interconnect," J. Semicond. **38**(10), 104004 (2017).